

Geophysical Research Letters®



RESEARCH LETTER

10.1029/2021GL097356

Greenland Ice Sheet Rainfall, Heat and Albedo Feedback Impacts From the Mid-August 2021 Atmospheric River

Jason E. Box¹ , Adrien Wehrlé² , Dirk van As¹ , Robert S. Fausto¹ ,
Kristian K. Kjeldsen¹ , Armin Dachauer¹ , Andreas P. Ahlstrøm¹ , and Ghislain Picard^{1,3} 

¹Geological Survey of Denmark and Greenland (GEUS), Copenhagen, Denmark, ²Institute of Geography, University of Zürich, Zürich, Switzerland, ³UGA, CNRS, Institut des Géosciences de l'Environnement (IGE), Grenoble, France

Key Points:

- A mid-August 2021 Greenland atmospheric river (AR) produced extreme ice sheet snow cover changes and high proglacial river discharge
- Surface heating from rainfall is small compared to latent and sensible heating, net longwave radiation or sunlight absorption
- Melt-albedo feedback enhanced upper elevations snow melt under clear skies following the heating delivered by the AR

Supporting Information:

Supporting Information may be found in the online version of this article.

Correspondence to:

J. E. Box,
jeb@geus.dk

Citation:

Box, J. E., Wehrlé, A., van As, D., Fausto, R. S., Kjeldsen, K. K., Dachauer, A., et al. (2022). Greenland ice sheet rainfall, heat and albedo feedback impacts from the mid-August 2021 atmospheric River. *Geophysical Research Letters*, 49, e2021GL097356. <https://doi.org/10.1029/2021GL097356>

Received 8 DEC 2021

Accepted 21 MAY 2022

Author Contributions:

Conceptualization: Jason E. Box
Data curation: Adrien Wehrlé, Robert S. Fausto, Ghislain Picard
Formal analysis: Jason E. Box, Dirk van As, Ghislain Picard
Funding acquisition: Robert S. Fausto, Andreas P. Ahlstrøm
Investigation: Jason E. Box, Adrien Wehrlé, Dirk van As, Ghislain Picard
Methodology: Jason E. Box, Kristian K. Kjeldsen, Ghislain Picard
Resources: Dirk van As, Robert S. Fausto, Andreas P. Ahlstrøm

Abstract Rainfall at the Greenland ice sheet Summit 14 August 2021, was delivered by an atmospheric river (AR). Extreme surface ablation expanded the all-Greenland bare ice area to near-record-high with snowline climbing up to 788 ± 90 m. Ice sheet wet snow extent reached 46%, a record high for the 15–31 August AMSR data since 2003. Heat-driven firn deflation averaged 0.14 ± 0.05 m at four accumulation area automatic weather stations (AWSs). Energy budget calculations from AWS data indicate that surface heating from rainfall is much smaller than from either the sensible, latent, net-longwave or solar energy fluxes. Sensitivity tests show that without the heat-driven snow-darkening, melt at 1,840 m would have totaled 28% less. Similarly, at 1,270 m elevation, without the bare ice exposure, melting would have been 51% less. Proglacial river discharge was the highest on record since 2006 for late August and confirms the melt-sustaining effect of the albedo feedback.

Plain Language Summary While rainfall at Summit station atop of the Greenland Ice Sheet in mid-August 2021 captured global attention, its direct surface thermal effects were weak and unable to explain the major melt and river discharge that occurred during and after the event. Exceptional heating of the ice sheet first occurred due to the heat transfer from condensation and the elevated air temperature during an atmospheric river (AR) episode. Satellite measurements reveal a rapid retreat of the snowline to higher elevations, exposing a large extent of relatively dark bare ice. Where snow remained, darkening due to wet snow metamorphism was responsible for sustained additional solar heating of the upper ice sheet elevations for the following 2 weeks. Observations from automatic weather stations and satellites, and river gauging, reveal that the AR had an immediate and sustained impact.

1. Introduction

On 14 August 2021, news headlines reported that rainfall was witnessed for the first time at Summit station near the highest point of the Greenland ice sheet (Ramirez, 2021) and was accompanied by high surface melt extent (Scambos et al., 2021).

Greenland rainfall can be delivered as part of concentrated poleward transport of moisture and heat in “atmospheric rivers” (ARs). Neff et al. (2014) identified ARs promoting Greenland melting by movement of air masses over the ocean with upstream development over the 2012 summer North American heatwave. The 2012 ARs were responsible for the largest observed single-day Greenland surface ice ablation rate of 0.28 m day^{-1} (Fausto, van As, Box, Colgan, & Langen, 2016; Fausto, van As, Box, Colgan, Langen, & Mottram, 2016; Mattingly et al., 2018). In addition to increasing Greenland rainfall fraction of precipitation (Niwano et al., 2021), the frequency of moist ARs reaching Greenland is also increasing (Mattingly et al., 2016), likely driven by more highly-amplified jet-stream patterns (Francis & Skific, 2015). ARs have strong surface energy budget (SEB) impacts (Mattingly et al., 2020), yet so far lack an analysis including on-ice rainfall observations.

Atmospheric heating induces snow darkening via snow grain metamorphism (Brun, 1989; Picard et al., 2012; Wiscombe & Warren, 1980) and dark bare ice exposure (Ryan et al., 2019; Wehrlé et al., 2021). Because snow grain growth occurs as a cube of liquid water content (Brun et al., 1992), small amounts of rain or meltwater can rapidly lower clean snow albedo with the observed cloud-free clean snow albedo range from 0.85 to 0.60 (Cuffey & Paterson, 2006). On glaciers, once snow ablates, the bare ice albedo can decline below the initial exposed bare ice albedo of 0.57 ± 0.11 (Wehrlé et al., 2021) to below 0.25 (van As et al., 2013) mainly from ice microbiological processes (Cook et al., 2020; Ryan et al., 2018; Stibal et al., 2017; Williamson et al., 2020). Thus, the Greenland

© 2022 The Authors.

This is an open access article under the terms of the [Creative Commons Attribution-NonCommercial License](https://creativecommons.org/licenses/by/4.0/), which permits use, distribution and reproduction in any medium, provided the original work is properly cited and is not used for commercial purposes.

Software: Jason E. Box, Adrien Wehrlé, Dirk van As
Validation: Jason E. Box, Adrien Wehrlé
Visualization: Jason E. Box, Adrien Wehrlé
Writing – original draft: Jason E. Box, Dirk van As, Kristian K. Kjeldsen, Andreas P. Ahlstrøm, Ghislain Picard
Writing – review & editing: Jason E. Box, Kristian K. Kjeldsen

ice sheet surface mass balance can be thought of as highly responsive through melt-albedo feedback (Flanner et al., 2011; Qu & Hall, 2007).

Here, surface glacial and proglacial hydrological impacts of the mid-August 2021 AR event are examined using Automatic Weather Station (AWS) records, satellite-derived wet snow and bare ice extents, snow and bare ice albedo, snowline elevation and proglacial meltwater river discharge data. A SEB model is used to quantify radiative, turbulent, and rainfall heat transfers for melting before, during and after the AR.

2. Data and Methods

2.1. AWS Meteorological Observations

AWS data from the Greenland Climate Network (GC-Net) (Steffen & Box, 2001; Steffen et al., 1996) and the Program for the Monitoring of the Greenland ice sheet (PROMICE) (Ahlstrøm & *PROMICE Project Team, 2008; Fausto et al., 2021) provide in-situ microclimatological observations. AWS albedo is computed using a running ± 11 -hr sum of upward/downward solar irradiance after (van den Broeke et al., 2004). New are Luftt WS401-UMB rain gauges initiated by GEUS starting June 2021 on GC-Net stations and from 2018 on the NUK_U PROMICE station. Rain gauge undercatch-correction and rainfall heat transfer details appear in Supporting Information S1.

2.2. Sentinel-3 Retrievals

Satellite retrievals of snow and ice (SICE) albedo are from the EU Copernicus Sentinel-3A Ocean Land Color Instrument (OLCI). These SICE albedo retrievals agree within 5% with the PROMICE AWS observations (Kokhanovsky et al., 2019, 2020). Cloud identification employs Sentinel-3A Sea and Land Surface Temperature Radiometer (SLSTR) data after (Metsämäki et al., 2015). The SICE algorithms and data appear in open access repositories (Box et al., 2020; Wehrlé et al., 2020).

2.2.1. Image Analysis

To increase clear sky coverage before and after the rain and AR event, we form average albedo mosaics; 9–13 August and 15–19 August 2021. From these, 100 m elevation-binned albedo averages are taken from three areas of interest (Figure 1b) and compared with AWS data. For estimates of average snowline position, we take the bare ice to snow albedo threshold of 0.565 after (Wehrlé et al., 2021).

2.3. Watson River Discharge and Catchment Surface Energy Budget

The Watson River, fed by a 11,922 km² catchment of the western Greenland ice sheet, has discharge recorded in Kangerlussuaq (van As et al., 2018) (see Figures 1 and S13 in Supporting Information S1). SEB data over the catchment are obtained from PROMICE KAN L, M, and U AWS data driving a SEB model (van As et al., 2017). The model solves for the surface temperature in balance with all energy fluxes: net shortwave and longwave radiation; sensible and latent heat fluxes; subsurface heat flux and rain heat flux. Turbulent heat fluxes are calculated using near-surface gradients in temperature, wind speed and humidity. Energy budget surplus contributes to melting for cases with surface temperature reaching 0°C.

2.4. AMSR Wet Snow Mapping

Advanced Scanning Microwave Radiometer (AMSR) AMSR-E and AMSR2 satellite 19 GHz passive microwave sensors are used to map the presence of snowpack water twice-daily (13 Universal Time Coordinate (UTC) ascending and 01 UTC descending passes) with 20 km spatial resolution after (Picard & Fily, 2006; Torinesi et al., 2003). Bare ice melting below the snowline is sometimes not captured by this algorithm and is ignored, leading to underestimates of the total ice sheet melt extent by up to 6%. The interannual frequency of wet snow is evaluated using the data span from years 2003–2021.

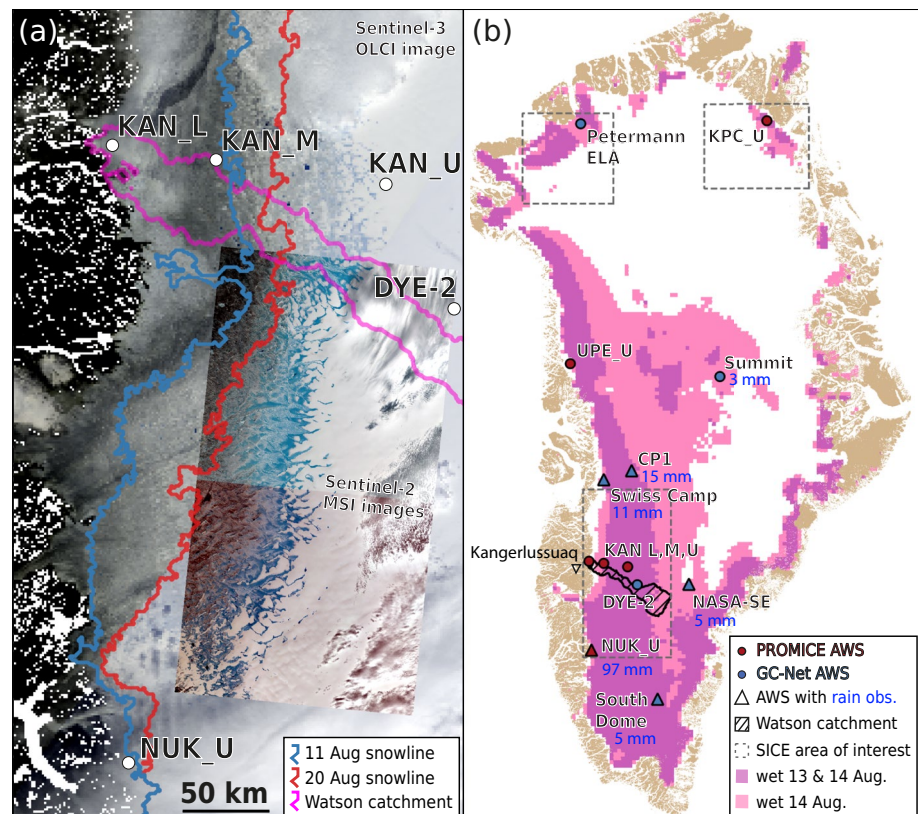


Figure 1. Automatic weather station (AWS) locations and the Watson River catchment appear on both panels. (a) An area of the western Greenland ice sheet on 20 August 2021 featured using a 1 km Sentinel-3 Ocean Land Color Instrument RGB image with inset 10 m Sentinel-2B true color images illustrating saturated snow and dark bare ice after the atmospheric river. (b) Greenland Climate Network and Program for the Monitoring of the Greenland ice sheet AWS locations and the expansion of wet snow area over 12-hr recorded by AMSR satellite passive microwave between August 13, 16 UTC and August 14, 04 UTC. Rain amounts at AWS are indicated and described further here and in Supporting Information S1.

3. Results and Discussion

3.1. Large-Scale Circulation

ERA5 850 hPa wind and water vapor fields (Copernicus Climate Change Service [C3S], 2017) (Figures S1a–S1c in Supporting Information S1) reveal a low-pressure system west of Greenland 13 August 2021 that drew an AR from the southwest onto the island by 14 August. By 16 August, another low had invaded which re-invigorated the southerly advection to Greenland as the AR shifted eastward. Southerly air and moisture delivery to southwest Greenland continued 17 August. By 19 August, the AR connection to Greenland had ceased and large-scale winds had reduced. On 20 August, the southerly flow was offshore from Greenland and weakened. By 21 and 22 August, northerly flow brought lower air temperatures to western Greenland with high pressure and clear sky conditions prevailing over the ice sheet. The relatively dry conditions continued through 27 August. Then, until 31 August, air temperatures continued decreasing across west Greenland with sustained northerly polar air advection, punctuating the ablation season.

3.2. Snow, Melt, Then Rain

All AWS with rainfall instruments (Figure 1) recorded air temperatures (T_{air}) exceeding 0°C at least 8 hours before rainfall. Prior to $T_{\text{air}} > 0^{\circ}\text{C}$ and rainfall, the AWS surface height and albedo records also indicate snowfall at several sites: CP1 (Figure S6b in Supporting Information S1); Summit (Figure S5a in Supporting Information S1); and NUK_U (Figures 2a and S4 in Supporting Information S1). Consistently, Sentinel-3 SICE retrievals indicate elevated albedo 11–13 August from snowfall prior to heating conditions.

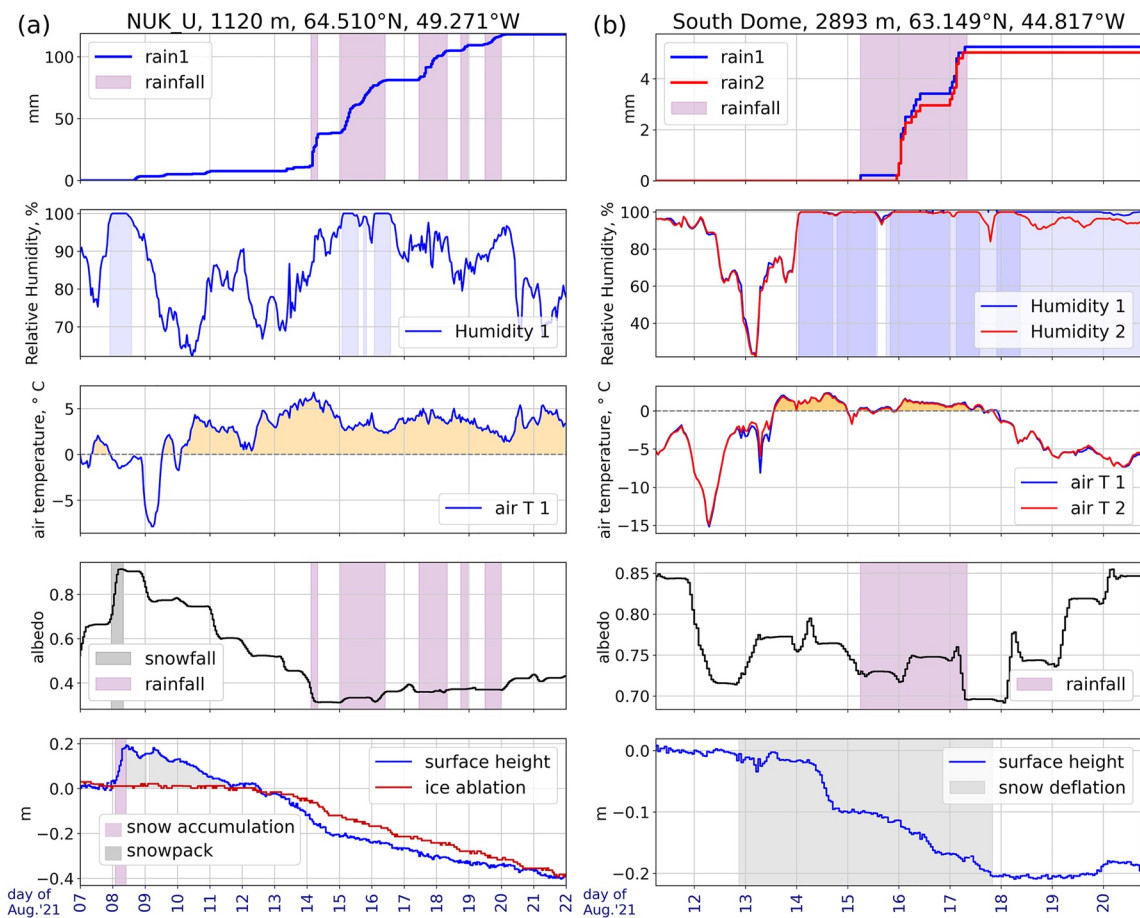


Figure 2. Rainfall, air temperature, albedo and surface height changes recorded by (a) the NUK_U Program for the Monitoring of the Greenland ice sheet (PROMICE) AWS (photo Figure S2 in Supporting Information S1) and (b) by the GEUS South Dome (SDM) Greenland Climate Network AWS photo (Figure S4 in Supporting Information S1). Note the differences in scale for the y-axes between sites. At SDM, instrument one is 1.2 m nearer the surface than instrument 2. Instrument heights start at roughly 2 m above ground. Shading is applied to the graphics to illustrate relative humidity cases above 98%, air temperature above 0°C, rainfall and snowfall cases. The NUK_U ice ablation recording is from a hydraulic sensor (Fausto et al., 2012).

3.3. AWS Site Rainfall, Albedo and Surface Height

3.3.1. NUK_U

Rainfall at NUK_U totaling 97.0 mm over three days (76 hr) commenced 14 August 04 UTC (UTC is hereafter “z”) and continued intermittently until 20 August 00z (Figure 2a). Four days before the AR, 0.18 m snow accumulated (07 August 23z–08 August 08z, 9h). The fresh snow had ablated prior to rainfall. The large (0.4) albedo decline caused by the AR includes bare ice exposure by 11 August. By the onset of rainfall 14 August, albedo stabilized below 0.4. Air temperatures peaked above 5°C when the highest rates of ice ablation occurred for times when rainfall is not recorded, net shortwave was relatively high ($>100 \text{ W m}^{-2}$) and net longwave was positive, indicative of low clouds. The NUK_U ice ablation during and after the AR totaled 0.4 m, substantial at 20% of the full 2008–2019 ablation season average.

3.3.2. South Dome

5.3 mm South Dome (SDM) rainfall was measured in three pulses during 50 hr from 15 August 06z–17 August 08z. The SDM record indicates snow deflation pausing when air temperatures drop below the melting point early 15 August (Figure 2b). Rainfall at this high elevation (2,893 m) location indicates the extremely high heat content of the air mass.

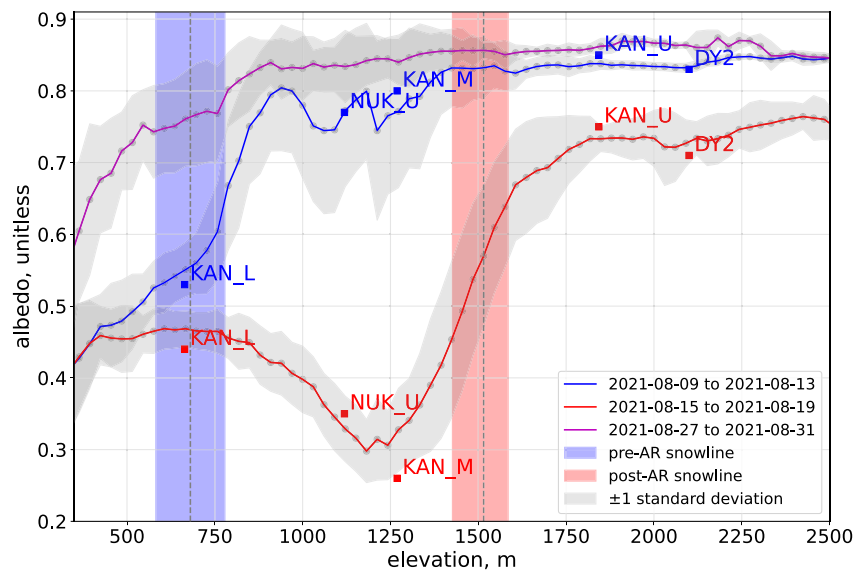


Figure 3. Averaged elevation profiles of snow and ice (SICE) albedo including the standard deviation of the values in the specified time interval and area of interest (Figure 1b). The albedo values from field observations are included for the before and after atmospheric river cases. The color shaded areas illustrate the ranges of the snowline using \pm one standard deviation from the SICE albedo and the 0.565 initial bare ice albedo after (Wehrlé et al., 2021).

3.4. Satellite Observations of Melt

At the onset of the AR 13 August, AMSR retrievals indicate a near-doubling of the ice sheet wet snow area to 9.99×10^5 km². The fractional melt area was 29% 13z 13 August, 44% by 01z 14 August, peaking at 46% at 13z on 14 August. If the bare ice area (BIA) below the snow limit is included, the peak melt extent was 51%.

AMSR recorded surface melting at Summit starting at 13z on 14 August. 12 hr earlier, no surface melting was detected in the vicinity of Summit (Figure 1b). Under the melting case at 16z, the Summit AWS (Figure S5a in Supporting Information S1) recorded very low (4 W m^{-2}) solar irradiance, indicating that surface heating is likely driven by turbulent sensible and condensational heat fluxes in addition to the downward longwave irradiance.

The average number of wet snow days for the whole ice sheet for the second half of August 2021 (4 days) was record-high for the AMSR period since 2003 and twice the 2003–2021 average.

It took 8 days, until 22 August, for the wet snow extent for the whole ice sheet to return to the pre-AR extent.

3.5. Atmospheric River Impacts on Snow and Ice Albedo

The AR conditions ablated the thin snow cover across the southwestern ablation area. At NUK_U (Figure S4 in Supporting Information S1) and KAN_M, an extreme albedo change (-0.4) is observed as snow ablation led to dark (albedo <0.4) bare ice exposure. Concurrently, within 4 days was a large (788 ± 90 m) snowline elevation increase across the western ice sheet area of interest (Figure 3). See also Figure 1b. The darkening can include the destruction of a sun crust (Tedstone et al., 2020) and water saturation of the surface (blue areas in Figures 1 and S11 in Supporting Information S1). Above snowline elevation, a SICE albedo drop by 0.10 ± 0.04 (Figure 3) is equivalent in magnitude with that observed by the KAN_U and DYE-2 AWS. In Arctic snow, where the concentration of light absorbing impurities (mainly black carbon) are typically very low (under 10 ng/g) (Doherty et al., 2013; Polashenski et al., 2015), the snow heating impacts are primarily attributable to snow grain growth and the albedo decline resulting from the grain growth-driven shortwave infrared darkening (Brun, 1989; Wiscombe & Warren, 1980).

The AR impacted the northern ice sheet with a snowline increase by 212 ± 60 m on average on the Humboldt Glacier, consistent with the GC-Net Petermann AWS station recording an albedo drop of 0.16 (Figure S7 in

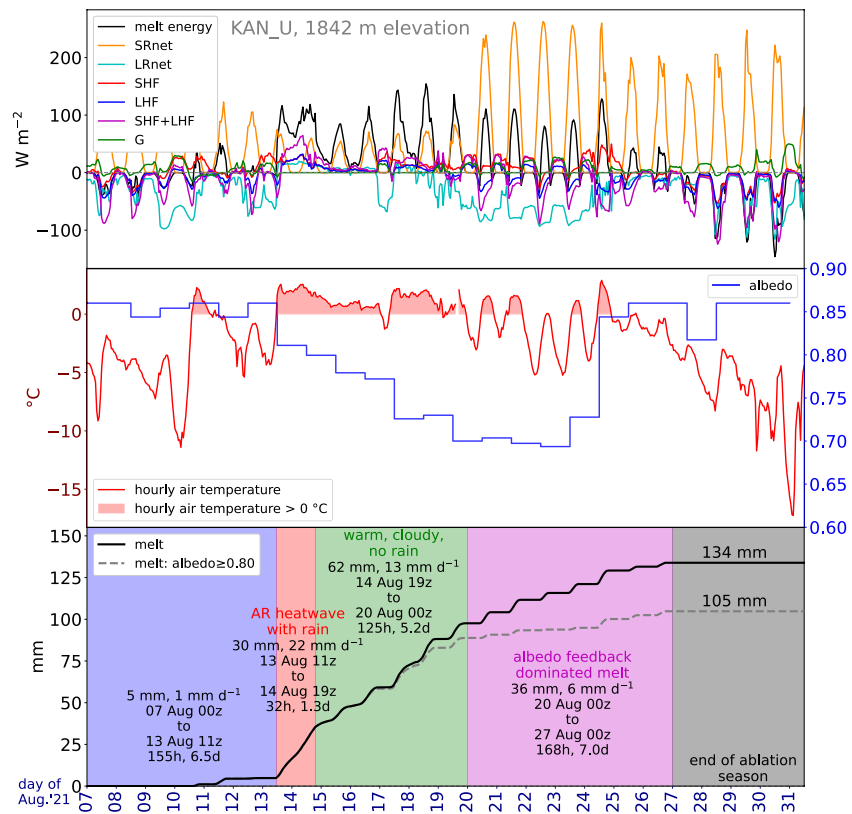


Figure 4. Surface energy budget and cumulative melting at 1,842 m elevation in the Watson River catchment (Figure 1) based on KAN_U AWS (See Figure S12 in Supporting Information S1) observations. Abbreviations: net shortwave radiation (SRNet); net longwave radiation (LRNet); sensible heat flux (SHF); latent heat flux (LHF); and ground conductive heat flux (G). The KAN sites lack rainfall observations.

Supporting Information S1). Similarly for the northeastern ice sheet, an average 121 ± 78 m snowline increase is evident in the SICE mosaics, consistent with the 0.12 albedo drop according to the KPC_U PROMICE AWS observations (Figure S8 in Supporting Information S1). The SICE albedo anomaly map illustrates widespread dark anomaly across and above much of the ice sheet ablation area, for example, on 22 August, including the northeastern ice sheet (Figure S9 in Supporting Information S1), likely including foehn effects (Mattingly et al., 2020).

3.6. Surface Energy Budget

From the start of the AR, a strong increase in downward net turbulent heat transfer from the heat and moisture import initiated melt (Figure 4 red shaded area). While a stronger melt increase is observed at lower elevations (see Figure S10 in Supporting Information S1), we feature a higher elevation site to highlight the AR impact over the much larger upper elevation accumulation area. During the AR prolongation phase (Figure 4, green area), while condensational and sensible heating and absorbed sunlight (SRNet) continue to fuel melt, key to the round-the-clock melting is the sustained positive net longwave radiation (LRNet) cf. Charalampidis et al. (2015), Van Tricht et al. (2016).

Daily average air temperature at KAN_U, 1,840 m above sea level, remained above melting around-the-clock 14–19 August. Subsequently, clouds began dissipating, indicated by negative trends in LRNet and turbulent fluxes (Figure 4). Yet, even as daily average T_{air} dropped below 0°C (Figure 4 purple shading), the snow albedo reduction initiated by melt during the AR and the resulting increase in net shortwave radiation (SRnet) sustained melting for five days (20–25 August). Similarly, Hofer et al. (2017) find cloud free conditions are important for the melt-albedo feedback. While some midday melting occurred, the only other surface melt energy source was a

minor ($<15 \text{ W m}^{-2}$) SHF. The cumulative melting during the melt-albedo feedback phase (Figure 4 purple area) was greater than during either the preceding AR “heatwave” or the “warm, cloudy, no rain” phases (Figure 4 green shading). Further, the rate of surface melting during the melt-albedo feedback phase was as large as the previous 5 days under more frequent cases of T_{air} above 0° , demonstrating the melt-albedo feedback. Were the sky conditions not mostly cloud-free, the feedback would have been less strong.

In a sensitivity calculation, by hypothetically inhibiting the snow-albedo feedback; keeping the KAN_U albedo ≥ 0.8 , we found a 28% reduced melting (broken gray line on the bottom panel of Figure 4). The approximation does not include (a) how in the brightened scenario, air temperature could drop during periods of no surface melting and (b) that effect could not feedback into all other SEB components like the turbulent sensible heat flux or subsurface energy fluxes. Further, penetration of shortwave radiation, neglected, yields minor warming of the snow pack that may enhance melt compared to our simulations, but it is difficult to quantify without a much more complex model (Dombrovsky et al., 2019; van Dalum et al., 2020).

The end of the ablation season is accompanied by a return of high albedo (>0.8) values (Figure 4) and melt termination. See also the 27–31 August snowline elevation profile in Figure 3.

3.7. Heat From Rainfall

At CPI, while the observed total rainfall (14 mm) is 62% as large as the melt from the SEB ($M = 23 \text{ mm}$), the calculated sensible heat transfer from the CPI rainfall amounts to just 2% the magnitude of M . Even if the rain temperature were somehow 1°C warmer, the rain contribution to surface melting would remain under 5%. Similarly, Garvelmann et al. (2014), Niwano et al. (2015) and Würzer et al. (2016) find that turbulent sensible and latent heat transfers dominate the SEB, under even heavier rainfall.

The five AWS sites recording rainfall (Figure 1) indicate another limiting factor for rainfall heating of the surface. Upward longwave irradiance indicated that the surface was already melting at the onset of rainfall. Therefore, any heat-driven snow grain growth would already have begun and would not require rainfall to occur.

At Summit, a photograph of a ca. 5 mm thick ice layer is featured (Ramirez, 2021). From this and taking the refrozen layer to have had a pre-melt snow density of 300 kg m^{-3} , we estimate a rainfall of 3.4 mm, which released 1.1 MJ m^{-2} of latent energy by refreezing with rain assumed at 0°C . As the water appears to have refrozen at the surface, this released energy probably radiated away upward as decreasing air temperatures ensued after the $\sim 8 \text{ hr}$ of $>0^\circ\text{C}$ conditions. Had this water percolated to depth, the released energy would have had a considerable snow warming impact because the latent heat release (by fusion) is more than an order of magnitude higher than the specific heat of water.

3.8. Bare Ice Area

The AR SEB variations in Figure 4 are evident in whole ice sheet BIA changes after Wehrlé et al. (2021). The $13,337 \text{ km}^2$ increase in BIA between 19 and 20 August 2021, right before cloudy conditions ended, was among the highest daily increase in BIA obtained by Sentinel-3 SICE retrievals in the five-year data set (2017–2021). The BIA anomaly during the AR is 30% above the five-year average and occurs 20 days later than the previous record BIA in 2019, consistent with the results from passive microwave (See Section 3.4).

3.9. Watson River Discharge

Starting 14 August, the day of the AR, Watson River discharge increased abruptly (Figure 5). River discharge and whole ice sheet BIA have a high correlation (0.858 , $1-p > 0.999$), suggesting the Watson River is representative of the ice sheet. The late August 2021 river discharge exceeded the observed (2006–2021) annual average peak and reached above any multi-day level in the 15–27 August period of record (Figure S13 in Supporting Information S1). River discharge remained elevated for 2 weeks after the AR arrival, more than the known routing delays for the catchment (van As et al., 2017), independently demonstrating the connection of the melt-albedo feedback amplification of the AR.

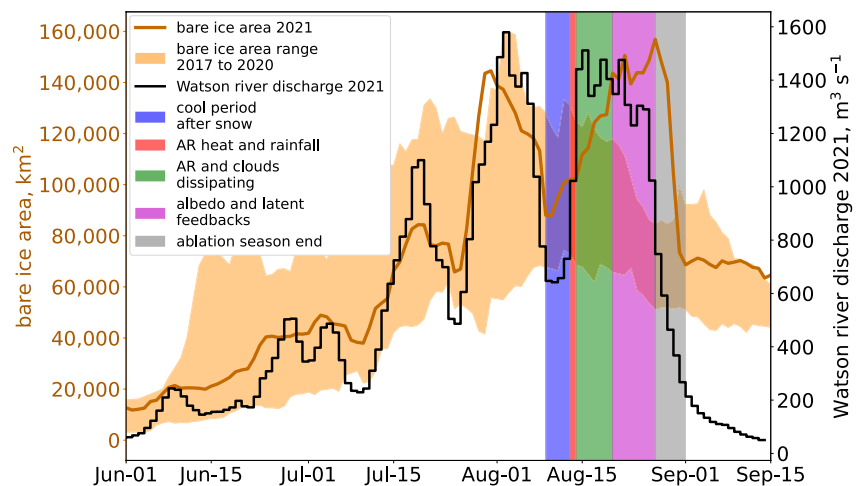


Figure 5. Greenland ice sheet bare ice area from Sentinel-3 after Wehrlé et al. (2021) and year 2021 Watson River discharge after (van As et al., 2018). Colored areas illustrate the different phases of the episode in Figure 4.

4. Conclusions

The mid-August 2021 AR produced widespread changes to snow cover extent and thickness and had strong glacio-hydrological impacts. The AR heatwave conditions were preceded by snowfall. The 2021 melt area and western river discharge was below average until the AR. However, with AR onset, a strong increase in surface turbulent sensible and latent (condensational) heat transfer to the surface drove extensive clearing of ablation area snow cover and rapid expansion of ice sheet surface melting. After clouds cleared 6 days later, the accumulation area snow albedo darkened by 0.1 from melt-driven wet snow metamorphism, sustaining melt conditions despite a return to sub-freezing air temperatures in early hours each day. Thus, the AR serves as a useful example of the melt-albedo feedback amplifying melt after a melt perturbation.

Satellite passive microwave data indicate how in the span of 12 hr, surface melting reached the ice sheet Summit at 04z 14 August, a time of day much more likely to be driven by turbulent than radiative fluxes. This single daily increase in wet snow extent for that late melt season date is the largest in the AMSR record from 2003.

The AR drove widespread snowline elevation increases; by 787 ± 122 m for the central western ice sheet, 212 ± 60 m for the far northwestern ice sheet (Humboldt and Petermann glaciers) and 121 ± 78 m for the northeastern ice sheet. The loss of ablation area snow cover drove the all-Greenland BIA to nearly as high in the extreme melt season of 2019. The BIA increase, between 19 and 20 August 2021, under cloudy conditions was among the highest daily increase in BIA obtained by Sentinel-3 in the first five-years of the mission.

During the AR, 0.14 ± 0.05 m firn area snow deflation is observed by four AWSs, with higher rates under non-rainy conditions, pointing to the relative dominance of turbulent surface heating.

Rainfall heat transfer contributed just 2% to the calculated melting at a 2,200 m elevation western ice sheet site (CP1 a.k.a. Crawford Point). Condensation or sensible heat transfer from the warm air mass was a far more powerful heat source. The observed amount of melting delivered by the AR could have happened without rainfall. Yet, the impacts of rain and meltwater refreeze are considerable provided that percolation delivers the melt below where the heat can be radiated away *and* that refreeze-at-depth occurs. We found no evidence for the latter condition because the rainfall amount was not extreme and the surface was already melting hours before the rainfall. Understanding any changes to the frequency and intensity of ARs appears to be a more important research target than the heat content of the liquid precipitation ARs may or may not produce. Further, while rainfall that does not percolate and refreeze may not have strong surface thermodynamic impacts, rainfall contribution to the hydraulics of Greenland ice (Doyle et al., 2015) may be more consequential to ablation through ice sheet flow acceleration.

The Watson River discharge for this period of August was the highest in the 16-year period of record since 2006 thus-far. The independent data from Watson River confirm the melt conditions initiated by the AR and sustained

by the melt-albedo feedback. The high correlation of the river discharge with BIA also highlights the importance of the lower ablation area in ice sheet freshwater discharge production.

As climate warming delivers more frequent cases of the 0°C melt boundary being passed, the resilience of the ice sheet to AR heating will become more compromised. Had the rain instead fallen as snow, the albedo feedback would have instead been both strongly toward minimizing surface energy absorption and increasing the meltwater retention capacity. So, even while the heat added by rain is small compared to other energy sources for melt, an increasing frequency of rainfall (instead of snowfall) can have a substantial future impact on the surface mass balance and as such is a strong indication of an amplified response of the ice sheet to the effects of warming.

Without the clear-sky conditions after the AR, the albedo feedback would have been less strong. The extent of albedo-feedback-perpetuated melt may well depend on whether the cloud cover was near the surface, providing a source of perpetuated melt through surface infrared heating, as compared to a situation with high clouds which could have had a relative cooling effect.

Data Availability Statement

SICE uses open source Dataverse Project software (“Dataverse Project,” 2021; King, 2007) for data curation at an open-access repository (Box et al., 2020) distributed under a non-restrictive license. Data to understand, evaluate, and build upon the reported research are available at <https://doi.org/10.22008/FK2/SKBAYA>.

References

- Ahlstrøm, A. P., & *PROMICE Project Team. (2008). A new programme for monitoring the mass loss of the Greenland ice sheet. *GEUS Bulletin*, 15, 61–64. <https://doi.org/10.34194/geusb.v15.5045>
- Box, J. E., Mankoff, K. D., Vandecrux, B., & Wehrle, A. (2020). SICE dataverse. *SICE Dataverse*. Retrieved from <https://dataverse01.geus.dk/dataverse/sice>
- Brun, E. (1989). Investigation on wet-snow metamorphism in respect of liquid-water content. *Annals of Glaciology*, 13, 22–26. <https://doi.org/10.3189/s0260305500007576>
- Brun, E., David, P., Sudul, M., & Brunot, G. (1992). A numerical model to simulate snow-cover stratigraphy for operational avalanche forecasting. *Journal of Glaciology*, 38(128), 13–22. <https://doi.org/10.3189/S0022143000009552>
- Charalampidis, C., van As, D., Box, J. E., van den Broeke, M. R., Colgan, W. T., Doyle, S. H., et al. (2015). Changing surface-atmosphere energy exchange and refreezing capacity of the lower accumulation area, West Greenland. *The Cryosphere*, 9(6), 2163–2181. <https://doi.org/10.5194/tc-9-2163-2015>
- Cook, J. M., Tedstone, A. J., Williamson, C., McCutcheon, J., Hodson, A. J., Dayal, A., et al. (2020). Glacier algae accelerate melt rates on the south-western Greenland ice sheet. *The Cryosphere*, 14(1), 309–330. <https://doi.org/10.5194/tc-14-309-2020>
- Copernicus Climate Change Service (C3S). (2017). *ERA5: Fifth generation of ECMWF atmospheric reanalyses of the global climate*. Retrieved from <https://cds.climate.copernicus.eu/>
- Cuffey, K. M., & Paterson, W. S. B. (2006). *The physics of glaciers*. Elsevier.
- Dataverse Project. (2021). *The Dataverse Project*. Retrieved from <https://dataverse.org/>
- Doherty, S. J., Grenfell, T. C., Forsström, S., Hegg, D. L., Brandt, R. E., & Warren, S. G. (2013). Observed vertical redistribution of black carbon and other insoluble light-absorbing particles in melting snow. *Journal of Geophysical Research*, 118(11), 5553–5569. <https://doi.org/10.1002/jgrd.50235>
- Dombrovsky, L. A., Kokhanovsky, A. A., & Randrianalisoa, J. H. (2019). On snowpack heating by solar radiation: A computational model. *Journal of Quantitative Spectroscopy & Radiative Transfer*, 227, 72–85. <https://doi.org/10.1016/j.jqsrt.2019.02.004>
- Doyle, S. H., Hubbard, A., van de Wal, R. S. W., Box, J. E., van As, D., Scharrer, K., et al. (2015). Amplified melt and flow of the Greenland ice sheet driven by late-summer cyclonic rainfall. *Nature Geoscience*, 8(8), 647–653. <https://doi.org/10.1038/ngeo2482>
- Fausto, R. S., Van As, D., Ahlstrøm, A. P., & Citterio, M. (2012). Assessing the accuracy of Greenland ice sheet ice ablation measurements by pressure transducer. *Journal of Glaciology*, 58(212), 1144–1150. <https://doi.org/10.3189/2012jog12j075>
- Fausto, R. S., van As, D., Box, J. E., Colgan, W., & Langen, P. L. (2016). Quantifying the surface energy fluxes in south Greenland during the 2012 high melt episodes using in-situ observations. *Frontiers of Earth Science*, 4, 82. <https://doi.org/10.3389/feart.2016.00082>
- Fausto, R. S., van As, D., Box, J. E., Colgan, W., Langen, P. L., & Mottram, R. H. (2016). The implication of nonradiative energy fluxes dominating Greenland ice sheet exceptional ablation area surface melt in 2012. *Geophysical Research Letters*, 43(6), 2649–2658. <https://doi.org/10.1002/2016gl067720>
- Fausto, R. S., van As, D., Mankoff, K. D., Vandecrux, B., Citterio, M., Ahlstrøm, A. P., et al. (2021). Programme for Monitoring of the Greenland Ice Sheet (PROMICE) automatic weather station data. *Earth System Science Data*, 13(8), 3819–3845. <https://doi.org/10.5194/essd-13-3819-2021>
- Flanner, M. G., Shell, K. M., Barlage, M., Perovich, D. K., & Tschudi, M. A. (2011). Radiative forcing and albedo feedback from the Northern Hemisphere cryosphere between 1979 and 2008. *Nature Geoscience*, 4(3), 151–155. <https://doi.org/10.1038/ngeo1062>
- Francis, J., & Skific, N. (2015). Evidence linking rapid Arctic warming to mid-latitude weather patterns. *Philosophical Transactions. Series A, Mathematical, Physical, and Engineering Sciences*, 373(2045), 20140170. <https://doi.org/10.1098/rsta.2014.0170>
- Garvelmann, J., Pohl, S., & Weiler, M. (2014). Variability of observed energy fluxes during rain-on-snow and clear sky snowmelt in a midlatitude mountain environment. *Journal of Hydrometeorology*, 15(3), 1220–1237. <https://doi.org/10.1175/JHM-D-13-0187.1>
- Hofer, S., Tedstone, A. J., Fettweis, X., & Bamber, J. L. (2017). Decreasing cloud cover drives the recent mass loss on the Greenland ice sheet. *Science Advances*, 3(6), e1700584. <https://doi.org/10.1126/sciadv.1700584>

Acknowledgments

This research was funded by the European Space Agency EO Sci for Society ESRIN CCN 4000125043/18/I-NB. GEUS field observations of rainfall have been supported by Greenland Integrated Observing System (GIOS) under the Danish Agency for Higher Education and Science, the INTAROS project under the European Union's Horizon 2020 research and innovation program under grant agreement No. 727890 and the Danish Ministry of Climate, Energy and Utilities via The Programme for Monitoring of the Greenland Ice Sheet (PROMICE) and the Greenland Climate Network (GC-Net). AGU data policy is followed with access to related data appearing in the data availability statement. We gratefully acknowledge PROMICE and GC-Net engineers: Alan Pedersen; Jakob Jakobsen; Chris Shields, field workers: Dirk van As; Andreas Ahlstrøm; Chris Shields; Nanna Karlsson; Alan Pedersen; Derek Houtz and Øyvind Winton and the Swiss Federal Institute for Forest, Snow and Landscape Research (WSL) data scientists: Ionut Iosifescu and Rebecca Kurup. Baptiste Vandecrux is thanked for commenting on the manuscript. Stefan Hofer and an anonymous referee provided useful constructive suggestions as external reviewers.

- King, G. (2007). An introduction to the dataverse network as an infrastructure for data sharing. *Sociological Methods & Research*, 36(2), 173–199. <https://doi.org/10.1177/0049124107306660>
- Kokhanovsky, A., Box, J. E., Vandecrux, B., Mankoff, K. D., Lamare, M., Smirnov, A., & Kern, M. (2020). The determination of snow albedo from satellite measurements using fast atmospheric correction technique. *Remote Sensing*, 12(2), 234. <https://doi.org/10.3390/rs12020234>
- Kokhanovsky, A., Lamare, M., Danne, O., Brockmann, C., Dumont, M., Picard, G., et al. (2019). Retrieval of snow properties from the Sentinel-3 ocean and Land Colour Instrument. *Remote Sensing*, 11(19), 2280. <https://doi.org/10.3390/rs11192280>
- Mattingly, K. S., Mote, T. L., & Fettweis, X. (2018). Atmospheric river impacts on Greenland ice sheet surface mass balance. *Journal of Geophysical Research*, 123(16), 8538–8560. <https://doi.org/10.1029/2018jd028714>
- Mattingly, K. S., Mote, T. L., Fettweis, X., van As, D., Van Tricht, K., Lhermitte, S., et al. (2020). Strong summer atmospheric rivers trigger Greenland ice sheet melt through spatially varying surface energy balance and cloud regimes. *Journal of Climate*, 33(16), 6809–6832. <https://doi.org/10.1175/JCLI-D-19-0835.1>
- Mattingly, K. S., Ramseier, C. A., Rosen, J. J., Mote, T. L., & Muthyala, R. (2016). Increasing water vapor transport to the Greenland ice sheet revealed using self-organizing maps: Increasing Greenland moisture transport. *Geophysical Research Letters*, 43(17), 9250–9258. <https://doi.org/10.1002/2016gl070424>
- Metsämäki, S., Pulliainen, J., Salminen, M., Luojus, K., Wiesmann, A., Solberg, R., et al. (2015). Introduction to GlobSnow Snow Extent products with considerations for accuracy assessment. *Remote Sensing of Environment*, 156, 96–108. <https://doi.org/10.1016/j.rse.2014.09.018>
- Neff, W., Compo, G. P., Martin Ralph, F., & Shupe, M. D. (2014). Continental heat anomalies and the extreme melting of the Greenland ice surface in 2012 and 1889. *Journal of Geophysical Research: Atmospheres*, 119(11), 6520–6536. <https://doi.org/10.1002/2014jd021470>
- Niwano, M., Aoki, T., Matoba, S., Yamaguchi, S., Tanikawa, T., Kuchiki, K., & Motoyama, H. (2015). Numerical simulation of extreme snow-melt observed at the SIGMA-A site, northwest Greenland, during summer 2012. *The Cryosphere*, 9(3), 971–988. <https://doi.org/10.5194/tc-9-971-2015>
- Niwano, M., Box, J. E., Wehrli, W., Vandecrux, B., Colgan, W. T., & Cappelen, J. (2021). Rainfall on the Greenland ice sheet: Present-day climatology from a high-resolution non-hydrostatic polar regional climate model. *Geophysical Research Letters*, 48(15). <https://doi.org/10.1029/2021gl092942>
- Picard, G., Domine, F., Krinner, G., Arnaud, L., & Lefebvre, E. (2012). Inhibition of the positive snow-albedo feedback by precipitation in interior Antarctica. *Nature Climate Change*, 2(11), 795–798. <https://doi.org/10.1038/nclimate1590>
- Picard, G., & Fily, M. (2006). Surface melting observations in Antarctica by microwave radiometers: Correcting 26-year time series from changes in acquisition hours. *Remote Sensing of Environment*, 104(3), 325–336. <https://doi.org/10.1016/j.rse.2006.05.010>
- Polashenski, C. M., Dibb, J. E., Flanner, M. G., Chen, J. Y., Courville, Z. R., Lai, A. M., et al. (2015). Neither dust nor black carbon causing apparent albedo decline in Greenland's dry snow zone: Implications for MODIS C5 surface reflectance. *Geophysical Research Letters*, 42(21), 9319–9327. <https://doi.org/10.1002/2015GL065912>
- Qu, X., & Hall, A. (2007). What controls the strength of snow-albedo feedback? *Journal of Climate*, 20(15), 3971–3981. <https://doi.org/10.1175/JCLI4186.1>
- Ramirez, R. (2021). Rain fell at the normally snowy summit of Greenland for the first time on record. *CNN*. Retrieved from <https://edition.cnn.com/2021/08/19/weather/greenland-summit-rain-climate-change/index.html>
- Ryan, J. C., Hubbard, A., Stibal, M., Irvine-Fynn, T. D., Cook, J., Smith, L. C., et al. (2018). Dark zone of the Greenland ice sheet controlled by distributed biologically-active impurities. *Nature Communications*, 9(1), 1065. <https://doi.org/10.1038/s41467-018-03353-2>
- Ryan, J. C., Smith, L. C., van As, D., Cooley, S. W., Cooper, M. G., Pitcher, L. H., & Hubbard, A. (2019). Greenland ice sheet surface melt amplified by snowline migration and bare ice exposure. *Science Advances*, 5(3), eaav3738. <https://doi.org/10.1126/sciadv.aav3738>
- Scambos, T., Stroeve, J., Koenig, L., Box, J. E., Fettweis, X., & Fettweis, X. (2021). *Rain at the summit of Greenland*. Retrieved from <http://nsidc.org/greenland-today/2021/08/rain-at-the-summit-of-greenland/>
- Steffen, K., & Box, J. (2001). Surface climatology of the Greenland ice sheet: Greenland climate Network 1995–1999. *Journal of Geophysical Research*, 106(D24), 33951–33964. <https://doi.org/10.1029/2001jd900161>
- Steffen, K., Box, J. E., & Abdalati, W. (1996). Greenland Climate Network: GC-net (No. 96–27). In S. C. Colbeck (Ed.) *Special Report on Glaciers, Ice Sheets and Volcanoes. Tribute to M. Meier*. CRREL.
- Stibal, M., Box, J. E., Cameron, K. A., Langen, P. L., Yallop, M. L., Mottram, R. H., et al. (2017). Algae drive enhanced darkening of bare ice on the Greenland ice sheet. *Geophysical Research Letters*, 44(22), 11463–11471. <https://doi.org/10.1002/2017GL075958>
- Tedstone, A. J., Cook, J. M., Williamson, C. J., Hofer, S., McCutcheon, J., Irvine-Fynn, T., et al. (2020). Algal growth and weathering crust state drive variability in Western Greenland ice sheet ice albedo. *The Cryosphere*, 14(2), 521–538. <https://doi.org/10.5194/tc-14-521-2020>
- Torinesi, O., Fily, M., & Genthon, C. (2003). Variability and trends of the summer melt period of Antarctic ice margins since 1980 from microwave sensors. *Journal of Climate*, 16(7), 1047–1060. [https://doi.org/10.1175/1520-0442\(2003\)016<1047:VATOTS>2.0.CO;2](https://doi.org/10.1175/1520-0442(2003)016<1047:VATOTS>2.0.CO;2)
- van As, D., Bech Mikkelsen, A., Holtegaard Nielsen, M., Box, J. E., Claesson Liljedahl, L., Lindbäck, K., et al. (2017). Hypsometric amplification and routing moderation of Greenland ice sheet meltwater release. *The Cryosphere*, 11(3), 1371–1386. <https://doi.org/10.5194/tc-11-1371-2017>
- van As, D., Fausto, R. S., Colgan, W. T., Box, J. E., & *PROMICE Project Team. (2013). Darkening of the Greenland ice sheet due to the melt albedo feedback observed at PROMICE weather stations. *GEUS Bulletin*, 28, 69–72. <https://doi.org/10.34194/geusb.v28.4728>
- van As, D., Hasholt, B., Ahlström, A. P., Box, J. E., Cappelen, J., Colgan, W., et al. (2018). Reconstructing Greenland ice sheet meltwater discharge through the Watson River (1949–2017). *Arctic Antarctic and Alpine Research*, 50(1), S100010. <https://doi.org/10.1080/15230430.2018.1433799>
- van Dalum, C. T., van de Berg, W. J., Lhermitte, S., & van den Broeke, M. R. (2020). Evaluation of a new snow albedo scheme for the Greenland ice sheet in the Regional Atmospheric Climate Model (RACMO2). *The Cryosphere*, 14(11), 3645–3662. <https://doi.org/10.5194/tc-14-3645-2020>
- van den Broeke, M., van As, D., Reijmer, C., & van de Wal, R. (2004). Assessing and improving the quality of unattended radiation observations in Antarctica. *Journal of Atmospheric and Oceanic Technology*, 21(9), 1417–1431. [https://doi.org/10.1175/1520-0426\(2004\)021<1417:AAITQO>2.0.CO;2](https://doi.org/10.1175/1520-0426(2004)021<1417:AAITQO>2.0.CO;2)
- Van Tricht, K., Lhermitte, S., Lenaerts, J. T. M., Gorodetskaya, I. V., L'Ecuyer, T. S., Noël, B., et al. (2016). Clouds enhance Greenland ice sheet meltwater runoff. *Nature Communications*, 7(1), 1–9. <https://doi.org/10.1038/ncomms10266>
- Wehrli, A., Box, J. E., Niwano, M., Anesio, A. M., & Fausto, R. S. (2021). Greenland bare-ice albedo from PROMICE automatic weather station measurements and Sentinel-3 satellite observations. *GEUS Bulletin*, 47. <https://doi.org/10.34194/geusb.v47.5284>
- Wehrli, A., Mankoff, K. D., Vandecrux, B., & Box, J. E. (2020). *SICE toolchain. Snow and ice (SICE) snow optical and microphysical retrievals from Sentinel-3*. Retrieved from <https://github.com/GEUS-SICE/SICE>

- Williamson, C. J., Cook, J., Tedstone, A., Yallop, M., McCutcheon, J., Poniacka, E., et al. (2020). Algal photophysiology drives darkening and melt of the Greenland ice sheet. *Proceedings of the National Academy of Sciences of the United States of America*, *117*(11), 5694–5705. <https://doi.org/10.1073/pnas.1918412117>
- Wiscombe, W. J., & Warren, S. G. (1980). A model for the spectral albedo of snow. I: Pure snow. *Journal of the Atmospheric Sciences*, *37*(12), 2712–2733. [https://doi.org/10.1175/1520-0469\(1980\)037<2712:amftsa>2.0.co;2](https://doi.org/10.1175/1520-0469(1980)037<2712:amftsa>2.0.co;2)
- Würzer, S., Jonas, T., Wever, N., & Lehning, M. (2016). Influence of initial snowpack properties on runoff formation during rain-on-snow events. *Journal of Hydrometeorology*, *17*(6), 1801–1815. <https://doi.org/10.1175/JHM-D-15-0181.1>

References From the Supporting Information

- Førland, E. J., Norske Meteorologiske Institutt, & Nordic Working Group on Precipitation (NWGP). (1996). *Manual for operational correction of Nordic precipitation data*. Norwegian Meteorological Institute. Retrieved from <https://www.worldcat.org/title/manual-for-operational-correction-of-nordic-precipitation-data/oclc/473734066>
- Goodison, B. E., Louie, P. Y. T., & Yang, D. (1998). *Solid precipitation measurement Intercomparison (No. 872)*. WMO.
- Li, X., & Kopp, R. (2019). *Wetbulb calculation*. Retrieved from <https://github.com/smartlxxx/WetBulb>
- Sevruk, B., Ondrás, M., & Chvíla, B. (2009). The WMO precipitation measurement intercomparisons. *Atmospheric Research*, *92*(3), 376–380. <https://doi.org/10.1016/j.atmosres.2009.01.016>
- Yang, D., Ishida, S., Goodison, B. E., & Gunther, T. (1999). Bias correction of daily precipitation measurements for Greenland. *Journal of Geophysical Research*, *104*(D6), 6171–6181. <https://doi.org/10.1029/1998jd200110>